Unveiling Tryptophan Dynamics and Functions Across Model Organisms via Quantitative Imaging

Kui Wang[1,6], Tian-lun Chen[1,6], Xin-xin Zhang[1,3,6], Jian-bin Cao[4,6], Pengcheng Wang[1,5], Mingcang Wang[4], Jiu-lin Du[1,2,3,8], Yu Mu[1,2,3,8], Rongkun Tao[1,7,8].

[1]*Institute of Neuroscience, State Key Laboratory of Neuroscience, Center for Excellence in Brain Science and Intelligence Technology, Chinese Academy of Sciences, 320 Yue-Yang Road, Shanghai 200031, China*

[2]*University of Chinese Academy of Sciences, 19A Yu-Quan Road, Beijing 100049, China*

[3]*School of Life Science and Technology, ShanghaiTech University, 319 Yue-Yang Road, Shanghai 200031, China*

[4]*Department of Anesthesiology, Taizhou Hospital of Zhejiang Province affiliated to Wenzhou Medical University, 150 Xi-men Road, Zhejiang 317000, China*

[5]*Department of Pediatric Cardiology, Xinhua Hospital, Shanghai Jiao Tong University School of Medicine, 1665 Kong-Jiang Road, Shanghai 200092, China*

[6]*These authors contributed equally to this work.*

[7]*Lead Contact*

[8]*Correspondence should be addressed to forestdu@ion.ac.cn, my@ion.ac.cn, rktao@ion.ac.cn*

ABSTRACT

Tryptophan is an essential amino acid involved in many cellular processes in vertebrates. Systemic and quantitative measurement of tryptophan is crucial for evaluating its essential role as a precursor of serotonin and kynurenine, key neuromodulators affecting neural and immune functions. We utilized a robust and highly responsive ratiometric indicator for tryptophan (GRIT) to quantitatively measure tryptophan dynamics in bacteria, mitochondria of mammalian cell cultures, and human serum. At the cellular scale, these analyses uncovered differences in tryptophan dynamics across cell types and organelles. At the whole-organism scale, we revealed that inflammation-induced tryptophan concentration increases in zebrafish brain led to elevated tryptophan metabolites serotonin and kynurenine levels, which is associated with the prolonged sleep duration. The reduction of zebrafish plasma tryptophan was mirrored in patients with inflammation symptoms and could serve as a biochemical marker of inflammation. In summary, this study introduces GRIT as a powerful method for studying tryptophan metabolism and functions across scales and species and suggests that tryptophan metabolic processes link the immune response and animal behavior.

INTRODUCTION

Tryptophan, an essential amino acid exclusively obtained from food, plays a crucial role in cellular protein synthesis and survival. Its absorption, transportation, and metabolic pathways within all vertebrates are highly conserved, leading to the production of various active molecules through pathways involving kynurenine, serotonin, and indole[1-3]. Thus, tryptophan metabolism serves as a pivotal metabolic regulator for processes such as immune responses, neural activities, and intestinal functions.

The tryptophan level metabolism is regulated at subcellular level, cell types, and across systems[4]. The abnormalities in tryptophan metabolism can induce systemic effects, influencing other tissues via the circulatory system, potentially triggering or exacerbating diseases like neurodegeneration, infections and cancer[5]. Moreover, tryptophan levels in plasma are closely associated with disease progression and prognosis in clinic[6]. Such extensive implications highlight the importance of systematically quantifying tryptophan dynamics across organisms.

Traditional methods, such as high-performance liquid chromatography (HPLC), are limited in revealing metabolic differences between different cell types and among subcellular compartments, also lack the precise temporal resolution to track rapid cellular metabolic changes during cellular stress[7]. In contrast, our recently developed genetically encoded tryptophan sensor, GRIT[8], represents a significant advancement over FRET-based tryptophan indicators (FLIPW-CTYT)[9]. GRIT offers a substantially larger dynamic range (9.55 versus 0.3), a smaller molecular size (39.7 kDa versus 80.1 kDa), and reduced photobleaching. These improvements make GRIT a highly effective tool for the quantitative measurement of tryptophan.

In this study, we demonstrate GRIT allows a new paradigm offering high spatiotemporal resolution, systematically quantifying dynamic changes in quantitatively mapping tryptophan dynamics in bacteria, mitochondria, zebrafish and human serum. Such advancements can facilitate a comprehensive understanding of the differences and dynamics in metabolite levels among cells within different tissues under physiological and pathological conditions, and reveals tryptophan metabolic processes link the immune response and animal behavioral

65   changes.

66

67   **RESULTS**

68   **Monitoring tryptophan dynamics in living bacteria**

69   Bacteria possess a tight regulatory mechanism on tryptophan metabolism[10]. We

70   investigated tryptophan uptake into *Escherichia coli* cells by expressing the GRIT sensor in

71   the cytoplasm (**Figures 1A and 1B**). Exogenous tryptophan addition induced a strong and

72   rapid fluorescence response in GRIT-positive bacteria, with a maximum ~3-fold increase

73   (**Figures 1B and 1C**), but not in GRITOL-expressing bacteria (**Figure 1B**). GRIT could

74   respond to 0.1 - 100 µM exogenous tryptophan in a dose-dependent manner with an

75   absorption rate of ~16.5 µM/s (**Table S1**). The Michaelis constant (K_m) of tryptophan uptake

76   (~0.58 µM) (**Figure 1D**) is similar to the reported biophysical properties of aroP (~0.4 µM)[11], a

77   tryptophan transporter that is highly expressed in bacteria according to the transcriptome[12]

78   (**Figure S1A**). The free concentrations of intracellular tryptophan in tryptophan deprivation and

79   tryptophan exposure conditions were measured to be 10.6 ± 3.7 µM (similar to the reported

80   level 12 µM[13]) and 192 ± 23.9 µM, respectively (**Table S1**). In addition, no significant

81   fluorescence change was observed when 19 other tested amino acids were added in the

82   absence or presence of tryptophan (**Figure S1B**). These results suggest that bacterial

83   tryptophan uptake is highly sensitive and specific.

84

85   **Detection of mitochondrial tryptophan dynamics in mammalian cells**

86   Mitochondria are semiautonomous subcellular organelles with their own genome and

87   require tryptophan transport from the cytosol to synthesize mitochondrial proteins. However,

88   due to the lack of specific detection methods, reports on mitochondrial tryptophan metabolism

89   have been sparse[14]. We selectively targeted the GRIT sensor in the mitochondrial matrix

90   (**Figures 2A and 2B**), resulting in a marked increase in fluorescence signals compared to the

91   control cells (**Figures S2A and S2B**). This enhancement enables effective fluorescence

92   measurement using both microplate readers and microscopy (**Figure 2A**). Mito-GRIT showed

93 an ~1.7-fold fluorescence increases upon the addition of 0.5 mM tryptophan (**Figure 2B**). The

94 mitochondrial tryptophan concentration was determined to be 112.4 ± 10.0 µM **(Table S1)**,

95 which was close to the HPLC measurements (108.0 ± 10.3 µM, **Table S1**). However, the

96 tryptophan uptake rate of mitochondria (~9.6 µM/min) was only ~18% of that in the cytoplasm

97 (~52.6 µM/min) (**Figure 2C, Table S1**). Upon tryptophan deprivation, the mitochondrial

98 tryptophan level was relatively stable in the first 20 min and decreased linearly at a rate of

99 ~0.8 µM/min (**Figure 2C, Table S2**). This suggests that the mitochondrial tryptophan pool is

100 predominantly regulated by cytosolic supply and the mitochondrial consumption, such as

101 protein synthesis.

102 We have demonstrated that cytosolic tryptophan pool is finely regulated by the supply of

103 external amino acids, which can be classified into three groups, Class I (large and neutral

104 amino acids, classic LAT1 substrate), Class II (five uncharged amino acids), Class III (six

105 charged or nonpolar amino acids)[8]. To further understand the characteristics of mitochondrial

106 tryptophan transportation, we detected mitochondrial tryptophan dynamics in response to all

107 other 19 amino acids. The six amino acids from Class III, which have no effect on cytosolic

108 tryptophan flux, also did not affect mitochondrial tryptophan dynamics (**Figures S2C-E and**

109 **Table S2**). In contrast, the 13 amino acids from Class I and Class II, despite their varied effects

110 on cytosolic tryptophan efflux, displayed similar impacts on mitochondrial tryptophan dynamics,

111 both in the absence or presence of tryptophan (**Figures S2C-E and Table S2**). Collectively,

112 the biophysical properties of mitochondrial tryptophan metabolism suggest specific and

113 unidirectional mitochondrial tryptophan transporters, which are different from the bidirectional

114 transportation of cell surface LAT1[8].

115

116 **Detection of serum tryptophan in patients with inflammation syndrome**

117 The clinical relevance of tryptophan metabolism lies in its association with various

118 diseases and inflammatory responses, particularly evident in the variations in serum levels[6].

119 Therefore, a rapid and efficient *in vitro* detection method could significantly advance diagnostic

120 technologies. We demonstrated that purified GRIT sensor could show large fluorescence ratio

121 changes to tryptophan ranging from 20 µM to 1 mM (**Figure S3A**). This broad detection range

122 is line with the theoretical prediction of an established web application "SensorOverlord"[15]

123 (**Figure S3B**), which overlaps with the concentration fluctuations of tryptophan in most

124 physiological and pathological conditions.

125   We collected serum samples from patients with inflammatory symptoms characterized by

126 following specific clinical criteria[16]: hypersensitive C-reactive protein (hs-CRP) concentration >

127 50 mg/L, and neutrophil ratio > 80%, white cell count > 10,000/μL (**Figure 3A**). We first

128 analyzed serum tryptophan levels using HPLC assay, followed by GRIT sensor detection of

129 the remaining portion of the same sample (**Figure 3A**). Despite the autofluorescence of blood

130 may interfere with the fluorescence assays, our results showed that GRIT sensor possess

131 much higher fluorescence signal than the serum background (**Figures S3C-F**). In addition,

132 the quantified tryptophan concentration was highly consistent between HPLC and GRIT

133 sensor measurements (**Figure 3B**), demonstrating the robustness of tryptophan

134 measurement with purified GRIT sensor in human serum samples. The serum tryptophan level

135 in inflamed patients (44.7 ± 4.7 μM) decreased ~25% compared with that of control (59.6 ±

136 3.6 μM) (**Table S1**). This reduction in serum tryptophan was consistently observed under

137 various conditions, including different sexes, ages, and extents of inflammation (**Figures 3C-**

138 **3F, S3G-I**). These results validate the GRIT sensor as an alternative high-throughput *in vitro*

139 diagnostic method and a decrease in serum tryptophan level could be a biochemical marker

140 of inflammation in patients.

141

142 **Detection of tryptophan metabolites and behaviors during inflammation in animal**

143 **model**

144   In the central nervous system, tryptophan is catabolized into serotonin and kynurenine,

145 both of which modulate neural activities and are related to sleep, depressive behaviors, and

146 fatigue symptoms[17-20]. To further explore the pathological implications of the documented

147 inflammation-triggered tryptophan redistribution phenomenon[8], we subsequently exposed

148 zebrafish to lipopolysaccharide (LPS). This resulted in a dose-dependent increase in sleep

149 duration (**Figures 4A-C and S4A**), consistent with the sustained elevation of tryptophan levels

150 in the brain following LPS treatment (**Figures S4B and S4C**). Next, we measured the

151 concentrations of tryptophan, serotonin, and kynurenine in isolated zebrafish brains. Inflamed

152 zebrafish showed a slight but non-significant increase in total tryptophan, a significant over 3-

153 fold increase in serotonin, and a 36% increase in the kynurenine, compared to control

154 individuals (**Figures 4D and 4E**). The rises of tryptophan metabolites in the brain may

155 contribute to the increased sleep behaviors during inflammation. Furthermore, inhibiting these

156 metabolic pathways resulted in developmental deformities, leading to their demise (**Figures**

157 **S4D and S4E**), suggesting that disrupting tryptophan metabolism leads to severe pathological

158 consequences.

159 In summary, our results demonstrate that inflammatory responses modulate tryptophan

160 levels across tissues (**Figure 4F**), with altered metabolic levels in the brain influencing

161 behavior. This indicates a metabolic link between the inflammatory response and animal

162 behavior.

163

164 **DISCUSSION**

165 In this study, we have demonstrated the versatility of using GRIT biosensor for

166 quantitatively measuring tryptophan levels across divers biological models, including bacteria,

167 subcellular organelles, and human serum. The GRIT, a superior genetically encoded tool,

168 supports multiple applications and long-term recordings of tryptophan.

169 Our findings show that intracellular tryptophan levels of different cell types and animal

170 models typically lie in the sub-millimolar range with distinct transportation properties

171 (**Supplementary Table 1**), which are in relevance to their specific functions in respective cells.

172 In *Escherichia coli*, tryptophan anabolism stands out as one of the most energy-intensive

173 metabolic pathways[21], which is activated exclusively under tryptophan deprivation conditions

174 (lower than sub-micromolar), along with a significant increase in its half-proliferation time[22].

175 The high affinity and rapid response to tryptophan facilitate rapid growth to adapt variable

176 environments[22] and allow gut microbes to continually metabolize tryptophan into indole

177 derivatives, influencing host the enteric nervous systems[23,24].

178 In mammal system, reprogramming tryptophan metabolism has become attractive for

179   tumor therapy, such as targeting LAT1 or indoleamine 2,3-dioxygenase (IDO)[5,25]. In contrast

180   to the bidirectional and rapid turnover of the cytosolic tryptophan pool, mitochondrial

181   tryptophan transportation exhibits a slower rate and higher specificity. The stringent regulation

182   of mitochondrial tryptophan pool may benefit protein synthesis and quality control within

183   mitochondria. Considering that the intense, ratiometric GRIT sensor is suitable for high-

184   throughput screening, it offers an opportunity to identify the mitochondrial transporter[26], and

185   an optical method and paradigm for studying the metabolism of subcellular organelles.

186   Quantitative measurements by GRIT sensor in intact animal and human serum could

187   reveal systemic tryptophan dynamics and its functions. Tryptophan metabolism regulates

188   immune systems and neural behaviors through kynurenine and serotonin pathways[5,19,27],

189   making the redistribution of tryptophan crucial for balancing the physiological functions under

190   pathological conditions[4,28]. Our measurements suggest that a flow of plasma tryptophan to the

191   brain and the consequent increase of tryptophan metabolites (serotonin and kynurenine)

192   during inflammation, resulted in prolonged sleep time in zebrafish. These results align with the

193   elevated serotonin concentration in the brain and fatigue and depression behaviors in LPS-

194   treated mice[29] and patients with inflammation symptoms, suggesting a potential metabolic link

195   between immune response and animal behavior[1,48].

196   *In vitro diagnostics* plays a pivotal role in disease detection, monitoring, and personalized

197   medicine, ultimately contributing to better patient outcomes and overall public health[30,31]. The

198   simple, fast and accurate GRIT probe allows high throughput quantification of tryptophan

199   concentrations in a patient's serum, which marks a significant advancement in the clinical

200   applications of fluorescent probes. The reductions in serum tryptophan levels during

201   inflammatory responses exhibit remarkable consistency between zebrafish and human

202   patients. Interestingly, a similar redistribution of tryptophan has been observed in

203   glioblastoma[32]. Moreover, our results suggest a correlation between patients' ages and serum

204   tryptophan levels (**Figures 3C, S3H and S3I**), but not with gender, implying a potential role of

205   tryptophan in aging, which are consistent with a previous report that tryptophan supplement

206   could extend worm lifespan via mitochondria NAD *de novo* synthesis[8]. These results

207   underscore the highly conserved nature of tryptophan metabolism and circulation among

208 vertebrates, emphasizing the relevance of our observations across different species.
209 Considering inflammation is a hallmark of various diseases, such as cancer, aging, obesity,
210 and cardiovascular disease, the systemic and quantitative measurement of tryptophan
211 dynamics on zebrafish offers new insights into the metabolic regulation mechanisms of these
212 diseases[4,5,33].

213 Overall, the systemic quantification of tryptophan metabolism with the GRIT sensor
214 portends the direct imaging of intracellular tryptophan metabolism and further understanding
215 of its functions under both physiological and pathological conditions. Quantitative imaging
216 paradigms in model animals is expected to pave the way for new therapeutic approaches in
217 human metabolic diseases.

218

219 **STAR METHODS**

220 Detailed methods of this paper include the following:

221 KEY RESOURCES TABLE

222 RESOURCE AVAILABILITY

223 Lead contact

224 Data availability

225 EXPERIMENTAL MODEL AND SUBJECT DETAILS

226 Cell cultures

227 Zebrafish

228 Human plasma samples

229 METHOD DETAILS

230 Plasmids construction

231 Cell culture, transfections, and establishment of stable cell lines

232 Fluorescence measurement of living cells with microplate reader

233 Fluorescence microscopy

234 *In vitro* transcription and mRNA purification

235 Zebrafish Sleep and Locomotion Analysis

236   Human plasma sample preparation

237   Quantitative measurement of tryptophan with GRIT sensor *in vitro* and *in vivo*

238   Tryptophan quantification with high performance liquid chromatography

239   Statistical Analysis
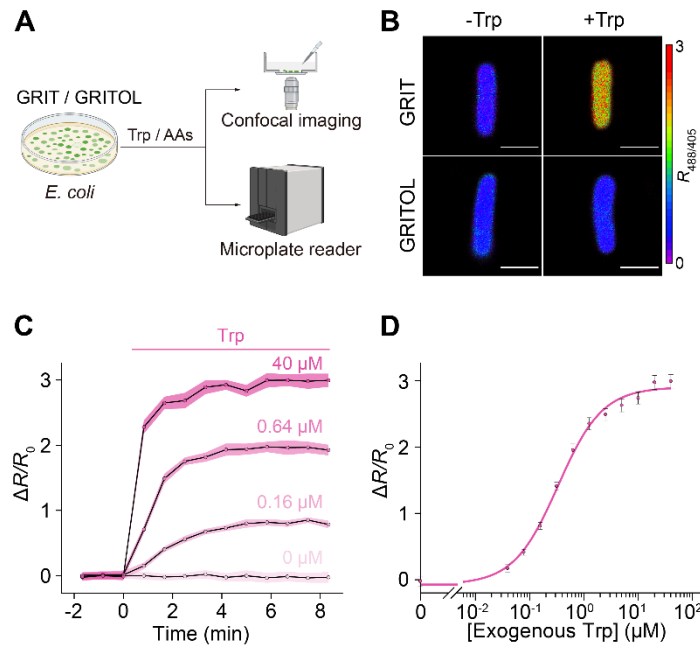
240

256

AUTHOR CONTRIBUTIONS

257

258   R.T. and Y. M. conceived the project. R.T., K. W., T. C., J. C. and X. Z. performed experiments. R.T., Y. M., K. W., T. C. and X. Z. analyzed data and made figures. R.T., Y. M. and J. D. wrote the draft and revised the manuscript.

261

DECLARATION OF INTERESTS

262

263   The authors declare no competing financial interests.

264

265

266

267

268

Figure 1. Detection of tryptophan uptake in bacteria with GRIT sensor. (A) Schematic representation illustrating the fluorescence detection of tryptophan (Trp) dynamics with the GRIT or GRITOL sensor in *Escherichia coli* cells. **(B)** Fluorescence images of bacteria expressing GRIT and GRITOL upon the addition of 0.1 mM Trp. **(C)** Changes in the fluorescence of GRIT in response to various concentrations of Trp in *Escherichia coli*. **(D)** The dose-response curve of GRIT-positive bacteria treated with exogenous Trp. Data are from panel Fig. 1C.

Scale bars, 1 μm. Data shown as mean ± s.e.m., n = 3 independent experiments in C and D. See also **Figure S1**, and **Table S1**.

278

279

280

281

282
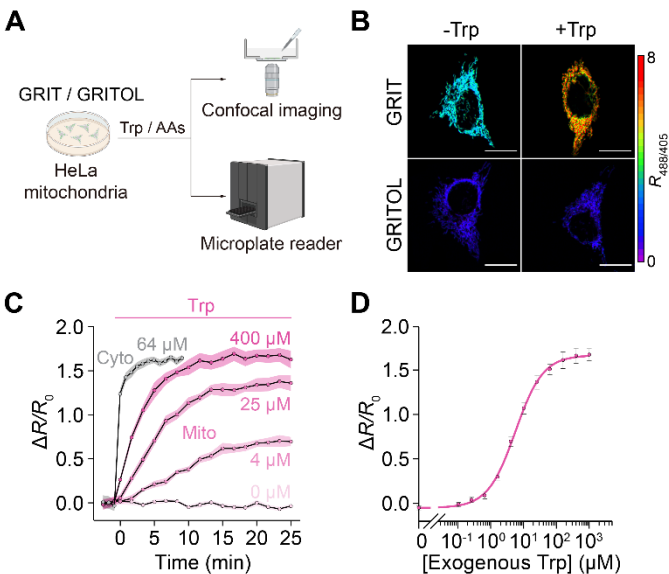
Figure 2. GRIT sensor reports mitochondrial tryptophan dynamics in cultured HeLa cells. (A) Schematic showing the fluorescence detection with mito-GRIT or mito-GRITOL sensor in HeLa cells. **(B)** Fluorescence responses of HeLa cells expressing GRIT (upper) and GRITOL (bottom) in mitochondria upon the addition of exogenous 0.5 mM Trp in HBSS buffer. **(C** and **D)** The traces (C) and dose-dependence curve (D) of mitochondrial GRIT sensor in response to varying concentrations of added tryptophan. The gray trace in C represents the fluorescence response kinetics of cytosolic GRIT to indicated Trp concentration (64 μM) in HBSS buffer, suggesting a significantly faster tryptophan uptake into the cytosol compared to the mitochondria.

Scale bars, 10 μm. Data shown as mean ± s.e.m. n = 3 independent experiments. See also **Figure S2** and **Tables S1, S2**.

294

295

296

297

298
299
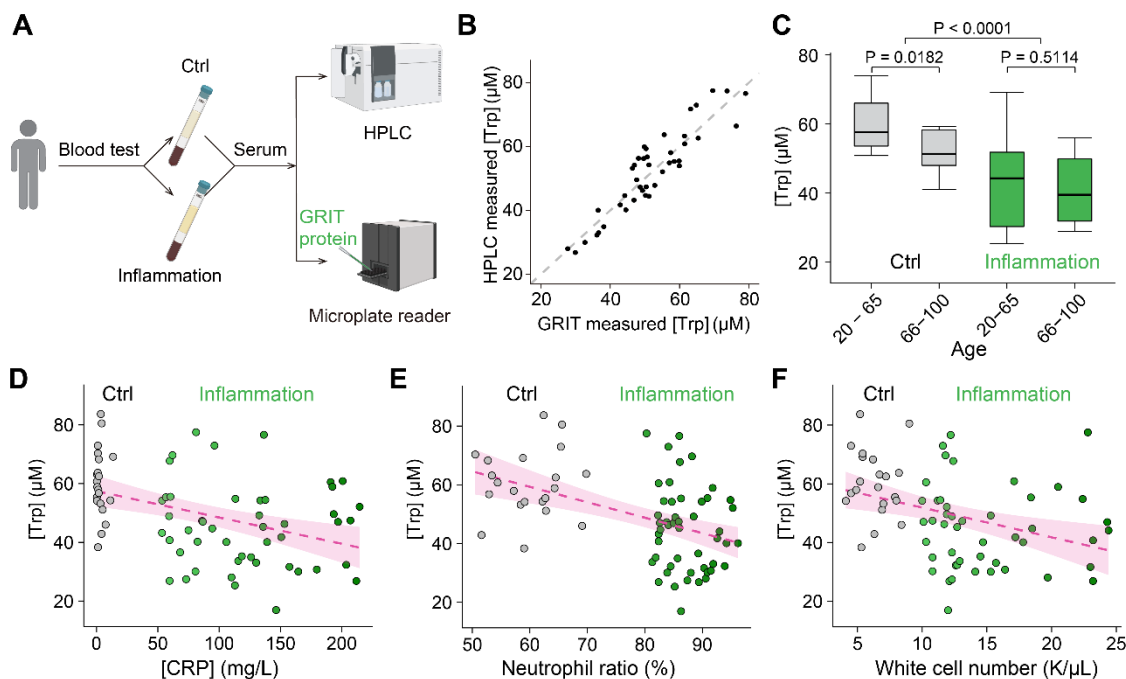
300 **Figure 3. Decreased serum tryptophan concentration is a biochemical mark of inflamed**
301 **patients**. **(A)** Schematic of the experimental procedures for the quantification of human serum
302 tryptophan. **(B)** A comparative analysis of quantitative serum tryptophan level in identical
303 samples measured by GRIT sensor assay or HPLC measurement (n = 42). **(C)** Tryptophan
304 concentrations of human serum samples in the control group (grey, n = 12 in 20-65 subgroup,
305 n = 13 in the 66-100 subgroup) and inflammation group (green, n = 17 in 20-65 subgroup, n =
306 35 in the 66-100 subgroup) based on age. Note that the total n number (42) in panel B are
307 smaller than the n number (77) in C, due to the volume of some serum samples were not
308 enough for GRIT sensor assay after HPLC (< 0.3 mL). **(D-F)** Relationships between tryptophan
309 concentrations in human serum samples and concentrations of hypersensitive C-reactive
310 protein (D), neutrophil ratio (E) and white cell number (F). The dashed magenta line represents
311 a linear fit of the data, with the shaded area indicating the fitting confidence interval.
312 Two-tailed student's unpaired t test for C. See also **Figure S3** and **Table S1**.

313
314
315
316

317

318

319
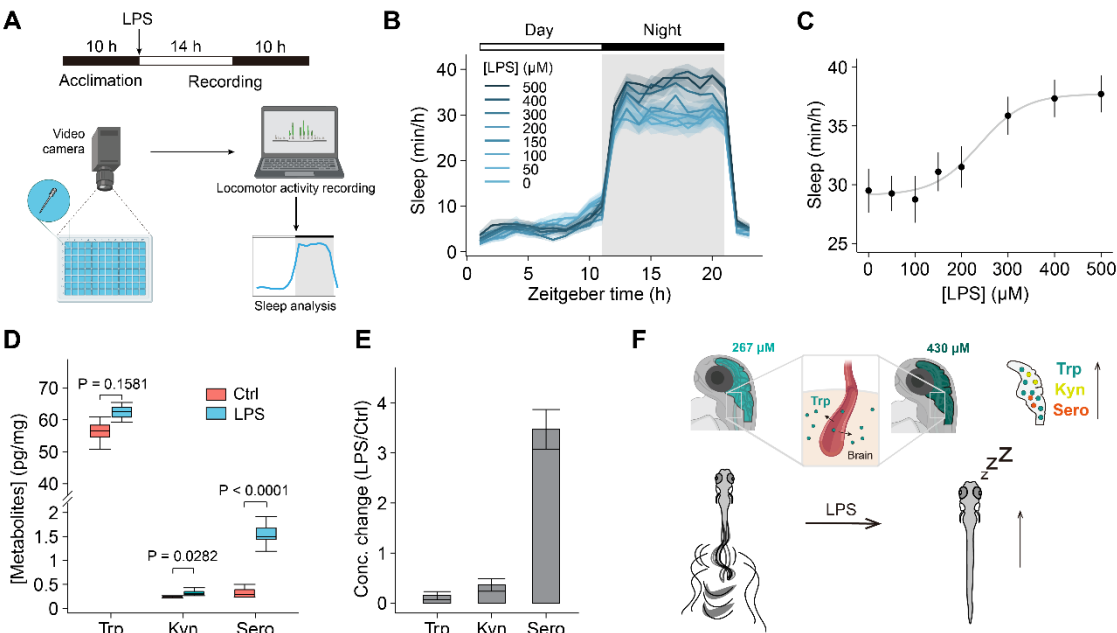
320 **Figure 4. Detection of metabolites levels in zebrafish larvae and zebrafish sleep**
321 **changes during inflammation. (A)** Schematic of the zebrafish sleep behavior measurement
322 during inflammation. **(B)** Changes in the sleep time of zebrafish in response to various
323 concentrations of LPS (n = 60 fishes from 5 - 7 independent experiments). LPS was added at
324 0 hr with indicated concentrations. **(C)** The dose-response curve of mean sleep time at night
325 of zebrafish treated with different concentrations of LPS. **(D-E)** The absolute levels (pg/mg)
326 (D) and relative changes (E) of tryptophan, kynurenine and serotonin in isolated zebrafish
327 brain with (n = 7) or without LPS treatment (n = 6). **(F)** The proposed working model of the
328 dynamics and functions of tryptophan in zebrafish during inflammation. During inflammation,
329 plasma tryptophan enters the brain, elevates the serotonin and kynurenine levels, and
330 increases zebrafish sleep time. The concentrations of brain tryptophan concentrations were
331 adapted from our previous study[8].
332 Data shown as mean ± s.e.m. Two-tailed unpaired student's t test for D. See also **Figures S4**.
333

334

335

336 **STAR METHODS**

337 **KEY RESOURECES TABLE**

REAGENT or RESOURCE	SOURCE	IDENTIFIER
Bacterial and Virus Strains		
Escherichia coli, JM109(DE3) strain	Weidi Biotech	EC1070M
Chemicals, and Recombinant Proteins		
PrimeSTAR Max DNA Polymerase	TaKaRa	R045B
Hieff Clone Plus One Step Cloning Kit	Yeasen	10912ES10
Lipopolysaccharides (LPS)	Beyotime	ST1470
DMEM (high glucose)	BBI	E600003
Fetal bovine serum (FBS)	ExCell Bio	FSS500
Lipofectamine 3000	Invitrogen	L3000015
T7 mMESSAGE mMACHINE kit	Invitrogen	AM1345M
Pancuronium dibromide	Selleck	S2497; CAS: 5500-66-0
Trypsin-EDTA	Gibco	25200072
HEPES	Sigma-Aldrich	H4034; CAS: 7365-45-9
Penicillin-Streptomycin Solution	BBI	E607011
Hieff Trans Liposomal Transfection Reagent	Yeasen	40802ES02
Puromycin	Beyotime	ST551
IPTG	Beyotime	ST098
Mitochondrial isolation kit	Beyotime	C3601
L-tryptophan	Sigma-Aldrich	T0254; CAS: 73-22-3
L-Glutamine	BBI	A100374; CAS: 56-85-9
L-Alanine	BBI	A600022; CAS: 56-41-7
L-Arginine	BBI	A600205; CAS: 74-79-3
L-Asparagine	BBI	A694341; CAS: 70-47-3
L-Aspartic acid sodium salt	BBI	A601178; CAS: 323194-76-9
L-Cysteine	BBI	A600132; CAS: 52-90-4
L-Glutamate	BBI	A602012; CAS: 142-47-2
L-Glycine	BBI	A110167; CAS: 56-40-6
L-Histidine	BBI	A604351; CAS: 71-00-1
L-Isoleucine	BBI	A100803; CAS: 73-32-5
L-Leucine	BBI	A100811; CAS: 61-90-5
L-Lysine	BBI	A110437; CAS: 657-27-2
L-Methionine	BBI	A100801; CAS: 63-68-3
L-Phenylalanine	BBI	A600991; CAS: 63-91-2
L-Proline	BBI	A600923; CAS: 147-85-3
L-Serine	BBI	A601479; CAS: 56-45-1
L-Threonine	BBI	A610919; CAS: 72-19-5
L-Tyrosine	BBI	A601932; CAS: 60-18-4
L-Valine	BBI	A600172; CAS: 72-18-4
Experimental Models: Cell Lines		
HeLa	Cell bank of Chinese	CSTR:19375.09.3101H

	Academy of Science	UMTCHu187
HEK293T	Cell bank of Chinese Academy of Science	CSTR:19375.09.3101H UMSCSP502
Experimental Models: Organisms/Strains		
Zebrafish, *Danio rerio*, *mitfa*[w2/w2]	Du Lab	N/A
Oligonucleotides		
5'_GATTCATTCTCTGGGAGGCATGGC CCAACAA TCACCCTATTC_3'; Forward primer for GRIT cloning into pcDNA3/hygro-mito	This paper	N/A
5'_GCTTAAGCTTTTATGCTAGATCGCT TTTCAGCAACAC_3'; Reverse primer for GRIT cloning into pcDNA3/hygro-mito	This paper	N/A
Recombinant DNA		
pcDNA3.1/hygro-mito-GRIT	This paper	N/A
pMD2.G	Trono Lab, addgene	https://www.addgene.org/12259/
psPAX2	Trono Lab, addgene	https://www.addgene.org/12260/
tol2-actin	Du Lab	N/A
Software and Algorithms		
FIJI	N/A	http://fiji.sc/
R (version 4.1.2)	R	https://www.r-project.org/
Rstudio (version 2022.02.0)	RStudio Team	https://www.rstudio.com/
Python (version 3.7)	Python Software Foundation	https://www.python.org/
Agilent MassHunter Qualitative Analysis Navigator (Version B.08)	Agilent	https://www.agilent.com/
FIQA code for fluorescent image quantitative analysis	This paper	N/A

338

RESOURCE AVAILABILITY

Lead contact

341   Further information and requests for resources and reagents should be directed to and

342   will be fulfilled by the Lead Contact, Rongkun Tao (rktao@ion.ac.cn).

343

Data availability

345   The data that supports the conclusions of this study are available from the corresponding

346   author upon request. GRIT and GRITOL constructs for mammalian expression are available

347   on the WeKwikGene plasmid repository at Westlake Laboratory, China

348   (https://wekwikgene.wllsb.edu.cn/). All other constructs are available upon requests.

349

EXPERIMENTAL MODEL AND SUBJECT DETAILS

Cell cultures

HeLa and HEK293T cell lines, obtained from the Cell Bank of the Chinese Academy of Science, were confirmed to be free of mycoplasma contamination. These cell lines were cultured in high glucose DMEM (BBI), supplemented with 10% FBS (ExCell Bio) and 1% penicillin-streptomycin (10,000 U/ml). The cells were maintained at 37 °C in a humidified atmosphere composed of 95% air and 5% CO_2.

357

Zebrafish

Colonies of Zebrafish (*Danio rerio*), specifically the Nacre strain (*mitfa*[w2/w2]), were maintained following standard procedures. The experimental protocols involving zebrafish were approved by the Chinese Academy of Sciences (Approval no. NA-046-2019). The zebrafish were kept under a light-dark cycle of 14 hours light to 10 hours dark, and the water temperature was consistently maintained at 28 °C.

364

Human plasma samples

All the population studied were from patients of Taizhou hospital of Zhejiang Province affiliated to Wenzhou Medical University. The experiments were performed according to the medical ethics rules (no. K20211202).

369

METHOD DETAILS

Plasmids Construction

For mitochondrial expression, the mitochondrial signal peptide from CoxVIII (cytochrome c oxidase subunit VIII) was duplicated and fused at the N-terminus of tryptophan biosensors[7]. To make lentiviral vectors, genes of mito-GRIT and mito-GRITOL were subcloned into pLVX-IRES-Puro backbone by NheI and PmeI.

376

Cell Culture, Transfections, and Establishment of Stable Cell Lines

To generate lentiviral particles, HEK293T cells were transfected with lentiviral plasmids,

379 including two packaging vectors (pMD2.G and psPAX2), using Hieff Trans (YEASEN).

380 Lentivirus-containing supernatants were collected at 48 and 72 hours post transfection and

381 subsequently applied to HeLa cells cultured in 6-well tissue culture plates supplemented with

382 8 μg/ml polybrene. Stable HeLa cell lines were established by cultivating the cells with 1 μg/ml

383 puromycin for one week, followed by sorting using MoFlo Astrios EQ (Beckman Coulter) with

384 a 488 nm laser line. The resulting stable HeLa cells were used for subsequent fluorescence

385 measurement experiments.

386

Fluorescence Measurement of Living Cells with Microplate Reader

388 Fluorescent bacteria cells were centrifugated at 4000 rpm for 2 min, followed by washing

389 three times with modified PBS buffer containing 10 mM HEPES, pH 7.3. The optical density

390 (OD_{600}) of bacterial suspensions was diluted to ~0.01, followed by a 30 min pre-starvation

391 before measurements. Three points were detected as the steady state, followed by addition of

392 different concentrations of tryptophan and a 10-min continuous reading on the BioTek

393 SynergyNeo Multi-Mode microplate reader. The fluorescence ratios ($R_{485/420}$) of GRIT and

394 GRITOL were divided to fit with titration curve for calibration.

395 The HeLa cell lines stably expressing GRIT sensors were trypsinized, resuspended and

396 plated in a black 96-well flat-bottom plate at a density of 26,000 cells per well, allowing them

397 to cultivate for 10-12 hours. Before the fluorescence measurements, the DMEM media was

398 removed, and cells were washed twice with freshly prepared HEPES buffer. Various amino

399 acids were then introduced into the detection buffer, each at specified absolute concentrations.

400 To correct the fluorescence values of GRIT sensors, the signals from HeLa cell samples were

401 background-subtracted.

402

Fluorescence Microscopy

404 Fluorescent bacteria cells were collected and diluted to the OD_{600} ~0.2 with modified PBS

405 buffer with or without 0.1 mM tryptophan. Bacteria solution (10 μL) was added on the 0.17 mm

406 coverslips (Nunc), then the coverslip was put upside down on a glass slide for imaging.

407 Cultured HeLa cells expressing Mito-GRIT and Mito-GRITOL were transferred to an 8-well

408 glass-bottomed dish (Cellvis) where the culture medium was replaced with HEPES buffer with

409 or without 0.5 mM tryptophan prior to experimentation. Utilizing an inverted confocal Olympus

410 FV3000 automatic microscope with a UPlanSApo 40 × Sil objective (N.A. 1.25), dual-excitation

411 ratio imaging was performed. The GRIT sensor was excited using 405 nm and 488 nm lasers,

412 capturing emission figures between 500-550 nm with a photomultiplier tube (PMT) in a

413 1024×1024 format and 12-bit depth. For subsequent data analysis, a semiautomatic analysis

414 was carried out using the FIQA code implemented in ImageJ Fiji. This analysis involved several

415 crucial steps, including background subtraction to eliminate unwanted noise, skin removal for

416 enhanced clarity, generation of ratiometric pseudocolored images to visualize variations, and

417 batch measurement of fluorescence intensities.

418

419 ### *In Vitro* Transcription and mRNA Purification

420 The mRNA preparation involved the utilization of a T7 mMESSAGE mMACHINE kit

421 (Invitrogen). We amplified the cDNAs corresponding to GRIT, GRITOL, or Tol2 and performed

422 *in vitro* transcription following the manufacturer's guidelines. To obtain purified mRNA, a two-

423 hour incubation in lithium chloride at -20 °C was performed, followed by dilution with DEPC-

424 treated nuclease-free water. This approach facilitated the generation of high-quality mRNA

425 samples for further experimental applications.

426

427 ### Zebrafish Sleep and Locomotion Analysis

428 Sleep analysis was performed based on tracking results of individual larval zebrafish.

429 Zebrafish larvae were raised with a light (14 hrs) and dark (10 hrs) cycle. The daytime starts

430 at 9 am and the night-time starts at 11 pm. When experiments started, individual larvae were

431 transferred into wells of a 96-well plate, which was placed inside Zebrabox (Viewpoint Life

432 Sciences, Lyon, France). Their locomotor activity was recorded using the quantization mode

433 in a video-tracking system (Viewpoint Life Sciences). Parameters for detecting different

434 movement patterns were determined empirically: detection thresholds, 15; burst, 29; freeze, 3;

435 bin size, 60 s. PBS or different doses of LPS were added into the bath at 9 am on the second

436 morning and maintained throughout the experiment.

437

438 ### Human Plasma Sample Preparation

439 Venous blood samples of patients were collected in tubes early in the morning, after an

440 overnight fast for a standard blood test, which are divided into control group and inflammation

441 group based on the blood test with clinical criteria[16]. For control group: (1) the number of white

442 cells is between 4,000 – 9, 000/μL; (2) the concentration of hypersensitive C-reactive protein

443 (hs-CRP) is less than 20 mg/L; (3) the neutrophil ratio is between 50% - 70%. For inflammation

444 group: (1) the number of white cell is over 10, 000/μL; (2) the concentration of hs-CRP is more

445 than 50 mg/L; (3) the neutrophil ratio is over 80%. The studied population consisted of 77 adult

446 subjects, which were randomly selected independent of gender and age. Selected plasma

447 samples were centrifuged at 3,500 rpm for 2 min and kept at 4 °C until analysis.

448

449 **Quantitative Measurement of Tryptophan with GRIT sensor *In Vitro* and *In Vivo***

450 Accurate and quantitative assessments of tryptophan levels in cells and serum samples

451 are achievable through the calculation of normalized sensor fluorescence ratios and comparing

452 these ratios with those obtained from purified GRIT protein in vitro, as described previously[8].

453 For the quantification of serum tryptophan concentrations with GRIT sensor, serum sample

454 was equally mixed with 1 μM GRIT or GRITOL sensor in 100 mM HEPES buffer, 100 mM KCl

455 (pH 7.3), followed by routine fluorescence measurement similar to protein titration experiments.

456 For quantification bacterial tryptophan, we measured the excitation fluorescence ratios of

457 cells expressing the GRIT sensor with or without 40 μM tryptophan as the intracellular

458 tryptophan levels in tryptophan-fed cells and tryptophan-starved cells, respectively. To account

459 for the pH effect, the excitation ratios of cells expressing GRIT were corrected by those of cells

460 expressing GRITOL measured in parallel and fitted with an *in vitro* protein titration curve at pH

461 7.3.

462 For *in situ* live-cell calibration, the unbound and saturated states of the mito-GRIT sensor

463 in HeLa cells could be approximated by treatment with 5 mM histidine and 0.5 mM tryptophan

464 in modified HEPES buffer (pH 7.4). The detection conditions were similar to those in live-cell

465 fluorescence measurements. The mitochondrial tryptophan levels were estimated by fitting

466 with purified protein titration curves at pH 8.0.

467

468 **Tryptophan Quantification with High Performance Liquid Chromatography**

469   HPLC method was used to accurate quantify intracellular tryptophan levels in HeLa cells.

470   We extracted the intracellular metabolites using 80% pre-cold methanol, evaporated the

471   supernatant, and dissolved the samples in 100 μL of 90% acetonitrile to remove proteins before

472   LC/MS quantification. The quantification process was carried out using a UHPLC system (1290

473   series; Agilent Technologies, USA) coupled with a quadruple time-of-flight mass spectrometer

474   (TripleTOF 6600, AB SCIEX, USA). The obtained results were analyzed using the Agilent

475   MassHunter Qualitative Analysis Navigator (B.08) software.

476   Mitochondria were extracted by a mitochondria isolation kit (Beyotime) and protein

477   concentration was quantified with a BCA kit (Mxbioscience LLC), followed by LC/MS

478   measurement. The protein amount was converted to mitochondria volume as reported [7].

479   The plasma tryptophan level was quantified with pre-column derivatization and reverse

480   phase ultra-performance liquid chromatography (RP-HPLC)[34]. In brief, protein was precipitated

481   by acetonitrile treatment in serum samples, and centrifuged at 13,000 rpm for 20 min.

482   Derivatization of the supernatant was carried out at 55 °C for 10 min, followed by separation

483   and quantitative analysis by external standard method with RP-HPLC.

484

485   **Statistical Analysis**

486   Data are presented as the mean ± s.e.m. from at least three experiments. All statistical

487   analyses and graphical representations were performed using R and Python. The figures were

488   compiled and finalized using Adobe Illustrator 2020.

489   The normality of the data was tested using the Kolmogorov–Smirnov test. For comparisons

490   between two groups, the two-tailed unpaired Student's t-test was employed for data with a

491   normal distribution in the majority of results, while the Mann-Whitney test was used for data

492   with a non-normal distribution. The specific sample size (n numbers) and P values of each

493   figure in the zebrafish and human serum sample experiments are listed in the corresponding

494   figures or legends.

495

REFERENCES

1. Cervenka, I., Agudelo, L.Z., and Ruas, J.L. (2017). Kynurenines: Tryptophan's metabolites in exercise, inflammation, and mental health. Science *357*. 10.1126/science.aaf9794.

2. Fernstrom, J.D., and Wurtman, R.J. (1972). Brain serotonin content: physiological regulation by plasma neutral amino acids. Science *178*, 414-416. 10.1126/science.178.4059.414.

3. Gheorghe, C.E., Martin, J.A., Manriquez, F.V., Dinan, T.G., Cryan, J.F., and Clarke, G. (2019). Focus on the essentials: tryptophan metabolism and the microbiome-gut-brain axis. Curr Opin Pharmacol *48*, 137-145. 10.1016/j.coph.2019.08.004.

4. Comai, S., Bertazzo, A., Brughera, M., and Crotti, S. (2020). Tryptophan in health and disease. Adv Clin Chem *95*, 165-218. 10.1016/bs.acc.2019.08.005.

5. Platten, M., Nollen, E.A.A., Rohrig, U.F., Fallarino, F., and Opitz, C.A. (2019). Tryptophan metabolism as a common therapeutic target in cancer, neurodegeneration and beyond. Nat. Rev. Drug Discov. *18*, 379-401. 10.1038/s41573-019-0016-5.

6. Xue, C., Li, G.L., Zheng, Q.X., Gu, X.Y., Shi, Q.M., Su, Y.S., Chu, Q.F., Yuan, X., Bao, Z.Y., Lu, J., and Li, L.J. (2023). Tryptophan metabolism in health and disease. Cell Metabolism *35*, 1304-1326. 10.1016/j.cmet.2023.06.004.

7. Tao, R.K., Zhao, Y.Z., Chu, H.Y., Wang, A.X., Zhu, J.H., Chen, X.J., Zou, Y.J., Shi, M., Liu, R.M., Su, N., et al. (2017). Genetically encoded fluorescent sensors reveal dynamic regulation of NADPH metabolism. Nat. Methods *14*, 720-728. 10.1038/nmeth.4306.

8. Tao, R., Wang, K., Chen, T.-l., Zhang, X.-x., Cao, J.-b., Zhao, W.-q., Du, J.-l., and Mu, Y. (2023). A genetically encoded ratiometric indicator for tryptophan. Cell Discovery *9*, 106. 10.1038/s41421-023-00608-1.

9. Kaper, T., Looger, L.L., Takanaga, H., Platten, M., Steinman, L., and Frommer, W.B. (2007). Nanosensor detection of an immunoregulatory tryptophan influx/kynurenine efflux cycle. PLoS Biol. *5*, e257. 10.1371/journal.pbio.0050257.

10. I P Crawford, a., and Stauffer, G.V. (1980). Regulation of Tryptophan Biosynthesis. Annu. Rev. Biochem. *49*, 163-195. 10.1146/annurev.bi.49.070180.001115.

11. Pittard, J., and Yang, J. (2008). Biosynthesis of the Aromatic Amino Acids. EcoSal Plus *3*. 10.1128/ecosalplus.3.6.1.8.

12. Sastry, A.V., Gao, Y., Szubin, R., Hefner, Y., Xu, S.B., Kim, D., Choudhary, K.S., Yang, L., King, Z.A., and Palsson, B.O. (2019). The Escherichia coli transcriptome mostly consists of independently regulated modules. Nat. Commun *10*. 10.1038/s41467-019-13483-w.

13. Bennett, B.D., Kimball, E.H., Gao, M., Osterhout, R., Van Dien, S.J., and Rabinowitz, J.D. (2009). Absolute metabolite concentrations and implied enzyme active site occupancy in Escherichia coli. Nat. Chem. Biol. *5*, 593-599. 10.1038/nchembio.186.

14. Hewton, K.G., Johal, A.S., and Parker, S.J. (2021). Transporters at the Interface between Cytosolic and Mitochondrial Amino Acid Metabolism. Metabolites *11*. 10.3390/metabo11020112.

15. Stanley, J.A., Johnsen, S.B., and Apfeld, J. (2020). The SensorOverlord predicts the accuracy of measurements with ratiometric biosensors. Sci Rep-Uk *10*. 10.1038/s41598-020-73987-0.

16. Brenner, D.R., Scherer, D., Muir, K., Schildkraut, J., Boffetta, P., Spitz, M.R., Le Marchand, L., Chan, A.T., Goode, E.L., Ulrich, C.M., and Hung, R.J. (2014). A review of the application of inflammatory biomarkers in epidemiologic cancer research. Cancer Epidemiol. Biomarkers Prev. *23*, 1729-1751. 10.1158/1055-9965.EPI-14-0064.

17. Oikonomou, G., Altermatt, M., Zhang, R.W., Coughlin, G.M., Montz, C., Gradinaru, V., and Prober, D.A. (2019). The Serotonergic Raphe Promote Sleep in Zebrafish and Mice. Neuron *103*, 686-701.e688. 10.1016/j.neuron.2019.05.038.

18. Oikonomou, G., Altermatt, M., Zhang, R.W., Coughlin, G.M., Montz, C., Gradinaru, V., and Prober, D.A. (2019). The Serotonergic Raphe Promote Sleep in Zebrafish and Mice. Neuron *103*, 686-701 e688. 10.1016/j.neuron.2019.05.038.

19. Schwarcz, R., Bruno, J.P., Muchowski, P.J., and Wu, H.Q. (2012). Kynurenines in the mammalian brain: when physiology meets pathology. Nat. Rev. Neurosci. *13*, 465-477. 10.1038/nrn3257.

20. Besedovsky, L., Lange, T., and Haack, M. (2019). The Sleep-Immune Crosstalk in Health and Disease. Physiol. Rev. *99*, 1325-1380. 10.1152/physrev.00010.2018.

21. Akashi, H., and Gojobori, T. (2002). Metabolic efficiency and amino acid composition in the proteomes of Escherichia coli and Bacillus subtilis. Proc Natl Acad Sci U S A *99*, 3695-3700. 10.1073/pnas.062526999.

22. Shehata, T.E., and Marr, A.G. (1971). Effect of nutrient concentration on the growth of Escherichia coli. J. Bacteriol. *107*, 210-216. 10.1128/jb.107.1.210-216.1971.

23. Ye, L.H., Bae, M., Cassilly, C.D., Jabba, S.V., Thorpe, D.W., Martin, A.M., Lu, H.Y., Wang, J.H., Thompson, J.D., Lickwar, C.R., et al. (2021). Enteroendocrine cells sense bacterial tryptophan catabolites to activate enteric and vagal neuronal pathways. Cell Host Microbe *29*, 179-196. 10.1016/j.chom.2020.11.011.

24. Gao, K., Mu, C.L., Farzi, A., and Zhu, W.Y. (2020). Tryptophan Metabolism: A Link Between the Gut Microbiota and Brain. Adv Nutr *11*, 709-723. 10.1093/advances/nmz127.

25. Lob, S., Konigsrainer, A., Rammensee, H.G., Opelz, G., and Terness, P. (2009). Inhibitors of indoleamine-2,3-dioxygenase for cancer therapy: can we see the wood for the trees? Nat. Rev. Cancer *9*, 445-452. 10.1038/nrc2639.

26. Qiu, Z.Z., Dubin, A.E., Mathur, J., Tu, B., Reddy, K., Miraglia, L.J., Reinhardt, J., Orth, A.P., and Patapoutian, A. (2014). SWELL1, a Plasma Membrane Protein, Is an Essential Component of Volume-Regulated Anion Channel. Cell *157*, 447-458. 10.1016/j.cell.2014.03.024.

27. Lemos, H., Huang, L., Prendergast, G.C., and Mellor, A.L. (2019). Immune control by amino acid catabolism during tumorigenesis and therapy. Nat. Rev. Cancer *19*, 162-175. 10.1038/s41568-019-0106-z.

28. Mondanelli, G., and Volpi, C. (2021). The double life of serotonin metabolites: in the mood for joining neuronal and immune systems. Curr. Opin. Immunol. *70*, 1-6. 10.1016/j.coi.2020.11.008.

29. O'Connor, J.C., Lawson, M.A., Andre, C., Moreau, M., Lestage, J., Castanon, N., Kelley, K.W., and Dantzer, R. (2009). Lipopolysaccharide-induced depressive-like behavior is mediated by indoleamine 2,3-dioxygenase activation in mice. Mol. Psychiatry *14*, 511-522. 10.1038/sj.mp.4002148.

30. Zou, Y., Wang, A., Huang, L., Zhu, X., Hu, Q., Zhang, Y., Chen, X., Li, F., Wang, Q., Wang, H., et al. (2020). Illuminating NAD(+) Metabolism in Live Cells and In Vivo Using a Genetically Encoded Fluorescent Sensor. Dev. Cell *53*, 240-252 e247. 10.1016/j.devcel.2020.02.017.

31. McRae, M.P., Rajsri, K.S., Alcorn, T.M., and McDevitt, J.T. (2022). Smart Diagnostics: Combining Artificial Intelligence and In Vitro Diagnostics. Sensors (Basel) *22*. 10.3390/s22176355.

32. Panitz, V., Koncarevic, S., Sadik, A., Friedel, D., Bausbacher, T., Trump, S., Farztdinov, V., Schulz, S., Sievers, P., Schmidt, S., et al. (2021). Tryptophan metabolism is inversely regulated in the tumor and blood of patients with glioblastoma. Theranostics *11*, 9217-9233. 10.7150/thno.60679.

33. Katsyuba, E., Mottis, A., Zietak, M., De Franco, F., van der Velpen, V., Gariani, K., Ryu, D., Cialabrini, L., Matilainen, O., Liscio, P., et al. (2018). De novo NAD(+) synthesis enhances mitochondrial function and improves health. Nature *563*, 354-359. 10.1038/s41586-018-0645-6.

34. Cevikkalp, S.A., Loker, G.B., Yaman, M., and Amoutzopoulos, B. (2016). A simplified HPLC method for determination of tryptophan in some cereals and legumes. Food Chem. *193*, 26-29. 10.1016/j.foodchem.2015.02.108.

586